Multiple-Time-Scale Motion in Molecularly Linked Nanoparticle Arrays

Christopher George,[†] Igal Szleifer,[†,‡,*] and Mark Ratner[†]

[†]Department of Chemistry and [‡]Department of Biomedical Engineering and Chemistry of Life Processes Institute, Northwestern University, Evanston, Illinois 60208, United States

ABSTRACT We explore the transport of electrons between electrodes that encase a two-dimensional array of metallic quantum dots linked by molecular bridges (such as α,ω alkaline dithiols). Because the molecules can move at finite temperatures, the entire transport structure comprising the quantum dots and the molecules is in dynamical motion while the charge is being transported. There are then several physical processes (physical excursions of molecules and quantum dots, electronic migration, ordinary vibrations), all of which influence electronic transport. Each can occur on a different time scale. It is therefore not appropriate to use standard approaches to this sort of electron transfer problem. Instead, we present a treatment in which three different theoretical approaches—kinetic Monte Carlo, classical molecular dynamics, and quantum transport—are all employed. In certain limits, some of the dynamical effects are unimportant. But in general, the transport seems to follow a sort of dynamic bond percolation picture, an approach originally introduced as formal models and later applied to polymer electrolytes. Different rate-determining steps occur in different limits. This approach offers a powerful scheme for dealing with multiple time scale transport problems, as will exist in many situations with several pathways through molecular arrays or even individual molecules that are dynamically disordered.

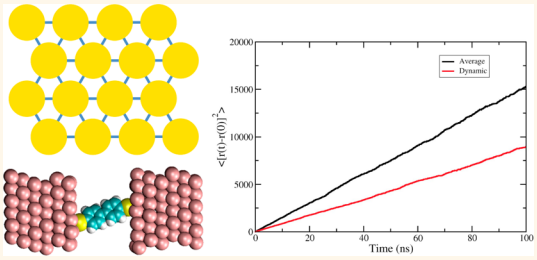

KEYWORDS: quantum dots · dynamic percolation · molecular conductance · electron hopping · electron transfer

Electron transfer (ET) is one of the most significant chemical processes. ET measurements are generally pursued in two physical limits. The most common examples comprise electron transfer either between two molecules or between two parts of a large molecule.[1−8] The molecular motions and solvent polarization combine to provide a polarization bath, within which electron tunneling occurs. In the nonadiabatic limit, the theory to understand the calculations of such reaction rates was first developed by Marcus, and depends upon the polarization coordinates providing a bath, that can absorb the excess energy for an exoergic reaction and provide the activation for an endoergic reaction.[9−13] The time scales in the nonadiabatic limit correspond to the electron tunneling time being substantially shorter than the characteristic bath dynamical times.

The second, far less common electron transfer phenomenon in molecules involves molecular transport junctions, in which (ideally) a single molecule is suspended between metallic electrodes, and the current across that molecular junction is measured as a function of voltage.[14−25] Here, the standard approach is the Landauer scheme,[15,18,19,21,23,26−29] in which the bath is now provided by the electronic sea in the electrodes. The dominant process here is elastic scattering, and the process is purely electronic—the molecules act as a tunneling bridge (at least in the off-resonance case), and charge tunnels between the macroscopic electrodes through the molecule.

Here we investigate a situation in which neither of these limits is appropriate. We consider molecules in junctions, existing in a quasi two-dimensional environment composed of metallic quantum dots with chain-like molecules that can bind to the dots at both ends (Figure 1). Molecular motion can change the interfacial structure, and therefore the electronic spectral density (a crucial component of Landauer theory) becomes time dependent.

* Address correspondence to igalsz@northwestern.edu.

Received for review July 14, 2012 and accepted December 1, 2012.

Published online December 02, 2012
10.1021/nn303320w

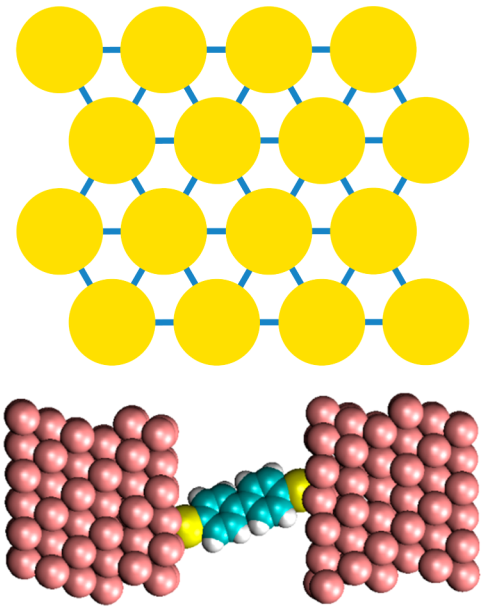

Figure 1. (Top) Schematic of nanoparticle array interlinked by molecular junctions. In the bottom panel, biphenyl dithiol is suspended between Au[111] electrodes. Gold atoms are purple, carbon are blue, hydrogens are white, and sulfurs are yellow.

We address these problems by combining tunneling calculations with molecular dynamics and kinetic Monte Carlo calculations. This is done to deal with the time-dependent evolution of molecular geometries, and with the multiple time scales involved in these systems.

The marriage of molecular electronics with nanostructured materials has proven fruitful in recent years, with the development of a variety of functional organic electronic devices. Supramolecular systems[30] as well as hybrid materials[31] have provided additional architectures with which to build and/or test molecular electronic devices. The potential advantages of such systems include better reproducibility, increased stability, and easier integration with traditional electronics. While nanostructured materials are a boon to the experimental development of molecular electronics, they require creative modeling techniques that treat time and length scales spanning several orders of magnitude, to capture the underlying physics dictating the electronic motion. In this work, we present a multiscale computational approach that underscores the importance of integrating multiple levels of theory when studying finite-temperature electron transport through nanostructured materials, in particular molecularly linked nanoparticle arrays.[32,33] Our computational method is used to probe a previously unexplored aspect of disorder in nanoparticle arrays. Specifically, we examine how structural fluctuations that occur on the atomic length scale and picosecond time scale affect transport on mesoscopic length scales and microsecond time scales.

Recent experimental efforts have demonstrated the utility of nanoparticle arrays as test-beds for molecular electronic junctions.[34−37] Single junctions can be formed by linking two macroscopic electrodes with dithiolated molecules or with other linkers[38−41] (Figure 1). By modifying the nature of the molecular interconnects, the arrays can be tuned to have varying levels of conductivity. This principle can be used to create switchable arrays by connecting nanoparticles with molecular linkers that exhibit photochromic or redox-sensitive conductance switching.[34,36] In such a system, it is possible to make qualitative inferences about the constituent junctions composing the array (when the array has a high conductance, more molecular switches are "on" than when the array has a low conductance). Extracting more specific information about individual junctions from conductance measurements of the array is a challenging task; it is necessary to understand the potential sources of disorder within the 2D structure that may be affecting electron transport across the array. For control of transport, such an undertaking is needed.

Well-studied sources of disorder include defects in the packing structure of the array, size dispersity of nanoparticles, and dynamic charging effects.[31,42,43] In addition to these issues, molecularly linked nanoparticle (NP) arrays will have disorder arising from structural fluctuations in the interconnecting molecular junctions. Junction conductance is highly dependent on the molecule/interface structure, and systems in which this geometry evolves over time can exhibit switching behavior.[44−46] While the speed and magnitude of the switching depend on the environment, the presence of stochastic switching is widely seen in junctions based on the Au−S binding motif, due partly to the labile thiol−gold bond.[47,48]

In this report, we explore the effect of stochastic switching in single-molecule junctions on the multiscale transport properties of molecularly linked nanoparticle arrays, using a combination of molecular dynamics (MD), an electron transport formalism based on Green's functions, and kinetic Monte Carlo simulations. Our results indicate that electronic motion through interlinked arrays may be described using dynamic bond percolation theory (DBPT), given the appropriate input parameters obtained from simulation, and when the switching can be described by a Poisson process.[49,50] For fluctuations that occur more quickly than the average electron hopping rate between nanoparticles, the dynamic effects average out. For slower fluctuations, electron mobility is gated by the dynamics of the interconnecting molecular junctions. Our findings highlight the importance of controlling molecule/interface geometric fluctuations in molecularly linked nanoparticle arrays. Additionally, they show the value of hierarchical computational approaches when modeling the electron transport properties of nanostructured materials.

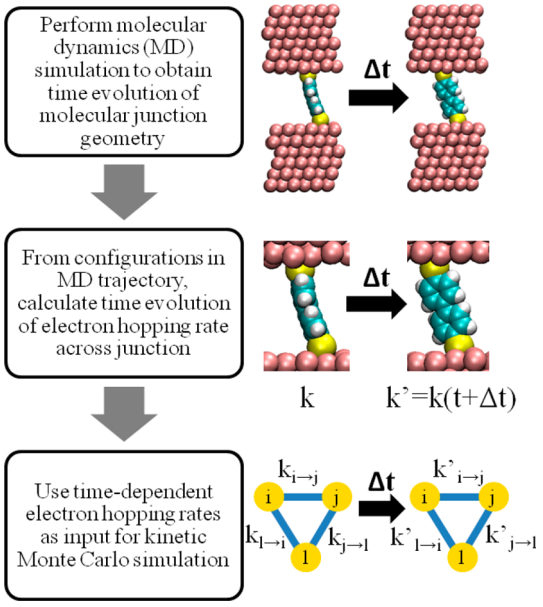

Figure 2. A flow-chart depiction of the multiscale computational approach used in this work.

COMPUTATIONAL HIERARCHY

An overview of the computational approach is shown in Figure 2. A description of the computational hierarchy will be given here, with additional details available in the Materials and Methods section. Three types of calculations were performed.

(1) In the MD simulations, a single biphenyl-4,4′-dithiol molecule is bound between two gold electrodes (Figure 1). The biphenyl is allowed to move, as are the three layers of Au atoms nearest to the junction. This setup is used to model the molecular junction formed between two neighboring nanoparticles. After every picosecond of simulation time, the configuration of the metal−molecule−metal junction is recorded.

(2) Conformations from the MD trajectory are then used as input for the next step in the computational approach, in which the transmission function at the Fermi energy $T(E_F,t)$ is computed for the geometry at time t. From the transmission function, the electron transfer rate $k_{i\rightarrow j}$ for thermally activated hopping between neighboring nanoparticles i and j can be calculated (see SI text):

$$k_{i\rightarrow j}(t) = \frac{2}{h}T(E_F, t)\frac{\Delta E}{e^{\Delta E/(k_B T)} - 1} \quad (1)$$

Here ΔE is the difference in energy in the electron transfer event, k_B is the Boltzmann constant, T is the temperature, and h is Planck's constant. The energy difference ΔE is approximated as a constant value for all simulations.

(3) The set of time-dependent hopping rates $\{k\}$ is then used in kinetic Monte Carlo (KMC) simulations. In the KMC simulations, electrons are allowed to hop between nearest-neighbor nanoparticles that are assembled in a hexagonal array. At the beginning of the KMC simulations, every bond between neighboring nanoparticles is assigned randomly a rate from the set $\{k\}$ obtained from steps 1 and 2. After every Monte Carlo step, each rate changes from $k_{i\rightarrow j}(t) \rightarrow k_{i\rightarrow j}(t + \Delta t)$ where Δt is the period at which configurations were recorded in the MD simulations (1 ps). In this way, we model the effect of the time evolution of the interconnecting molecular linkers. Upon completion of the KMC simulations, the electronic diffusion coefficients are computed from the average electronic mean squared displacements.

Within this multiscale approach, each of the three steps is necessary. The MD simulations provide information regarding the structural fluctuations of the interparticle molecular bridges, the quantum transport calculations relate those geometrical fluctuations to changes in the interparticle electron transfer rates, and the KMC simulations reveal the effect of the fluctuations on mesoscopic transport. Using this framework, we can understand the effect that fluctuations in the molecular junctions have on electronic motion through the array.

RESULTS

Because surface defects can play an important role in the geometric and transport properties of molecular junctions,[51] two types of electrode structures are considered: electrodes with defect-free surfaces, and electrodes with $^2/_3$ of the surface atoms missing. We will examine the defect-free surfaces first (Figure 1). In the system with defect-free surfaces, the most dramatic structural changes in the junction are a result of the mobility and intramolecular motion of the biphenyl molecule. The labile Au−S bond permits diffusion of the biphenyl dithiol within the junction, allowing the molecule to access a range of binding locations and tilt angles, which affect the transport properties.[52−54] In addition to the variety of binding geometries, the biphenyl experiences a number of conformational changes which also affect transport through the junction.[54] The time-dependent transmission function distribution is shown in Figure 3a with a histogram of transmission values in Figure 3b. The average value of the transmission is 0.008 ± 0.002 corresponding to a characteristic hopping time of 12 ps (from eq 1, assuming ΔE = 10 meV). Fluctuations in the time-dependent transmission values occur more rapidly than the characteristic hopping time, with no long-lived stochastic switching observed. As predicted from previous theoretical and experimental studies,[55,56] the histogram of transmission values exhibits a log-normal distribution.

After performing the KMC simulations using the time-dependent rates calculated from eq 1, the average electronic mean squared displacement can be computed (red curve in Figure 4). The linearity of the curve indicates normal diffusion, and the diffusion coefficient can be calculated from the slope of

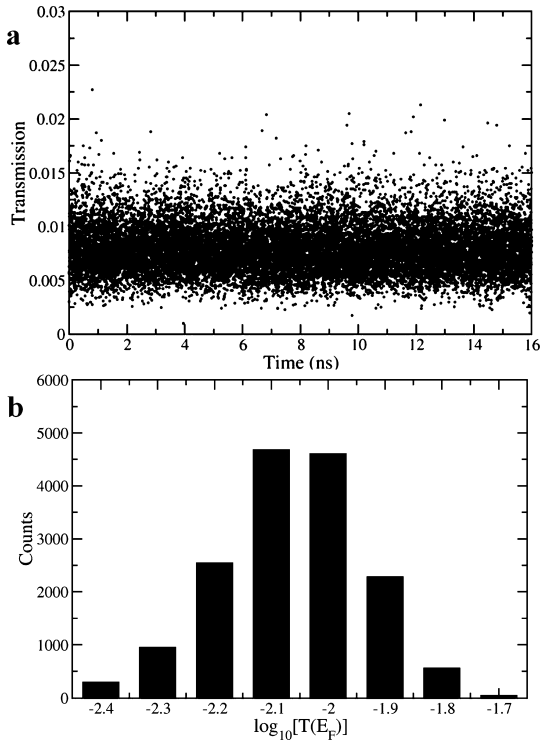

Figure 3. (a) Time-dependent transmission and (b) log-normal histogram of transmission values. Transmission values fluctuate rapidly and follow a unimodal distribution.

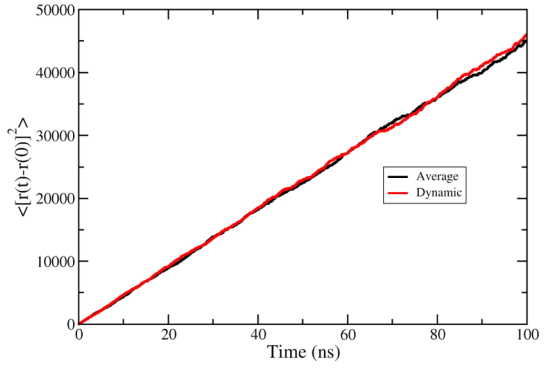

Figure 4. Electronic mean squared displacements (MSD) as a function of time for the system with ordered electrodes. The "dynamic" curve (red) is computed using the hierarchy described in Figure 2. The "average" curve (black) is calculated assuming that all electron hopping rates are equivalent to the average hopping rate from the "dynamic" simulation. The equivalent slopes indicate that the fluctuations in the "dynamic" simulation have little effect on the mesoscopic transport through the array. Units of distance are defined by the separation between nearest-neighbor nanoparticles.

the curve. To evaluate the effects of fluctuations on the overall electronic diffusion, KMC simulations were performed in which all interparticle hopping rates were held constant at the rate calculated from eq 1 using $T(E_F,t) = T(E_F)_t = 0.008$. The average electronic mean squared displacement for this simulation is shown in Figure 4 (black curve). The slopes for the two curves are essentially identical, indicating that the rapid geometric fluctuations have a negligible effect on the mesoscopic transport properties of the nanoparticle array. The actual diffusion coefficient $D \equiv \langle r^2 \rangle/(4t) = 112\ l^2/(n\,\mathrm{sec})$, here l is separation between nearest neighbor nanoparticle centers. For a typical spacing $l \cong 10$ nm, this yields $D \cong 10^{-1}$ cm^2/sec.

The computational procedure is repeated for a system in which $^2/_3$ of the atoms in the first surface layer are removed from each electrode. Molecular dynamics simulations are performed as before, and time-dependent transmission values and a histogram of transmission values are calculated (Figures 5a,b). Dramatically different transport properties appear in this case. The time-dependent transmission shows distinct switching events (or equivalently, long-lived fluctuations) in which the junction changes between a low-transmission (low-T) and high-transmission (high-T) state. The low-T/high-T ratio is approximately 0.003. This switching is also apparent in the histogram of transmission values (Figure 5b) which is best described by a bimodal distribution, in contrast to the unimodal distribution seen in Figure 4b. The underlying change in geometry that causes the switching to occur is shown in Figure 5c,d. In Figure 5c, the molecule is in approximately the middle of the junction, adsorbed above islands of gold surface atoms on either side. This corresponds to a high-transmission state. In Figure 5d, the molecule is in a low-transmission state. Here, the biphenyl is adsorbed closely to only one electrode with one of the sulfur atoms embedded in an island of gold atoms.

The average electronic mean squared displacements are shown in Figure 6. As before, we test the effect of the fluctuations by performing KMC simulations in which all hopping rates are held constant at the rate computed using the average transmission $T(E_F,t) = T(E_F)_t = 0.002$. In contrast to Figure 4, the mean squared displacement computed from the average rate (Figure 6, black curve) has a dramatically different slope compared with the curve computed from the time-dependent rates (red curve). For this system, the geometric fluctuations do have a significant effect on the electronic diffusion through the nanoparticle array.

We propose that the crucial difference between the fluctuations in the system with an ordered electrode surface versus disordered electrode surface is the temporal longevity of low-transmission and high-transmission states. At first glance, the fluctuations appear to occur very rapidly in both systems: traditional single molecule junction measurements would not be able to resolve either because even the so-called "long-lived" switching events occur on the nanosecond time scale. However, the temporal parameter that defines "fast" or "slow" in a network of molecular junctions is the characteristic interparticle electron hopping time. If fluctuations occur more quickly than the characteristic hopping time (shorter in the first system than in the second) the fluctuations

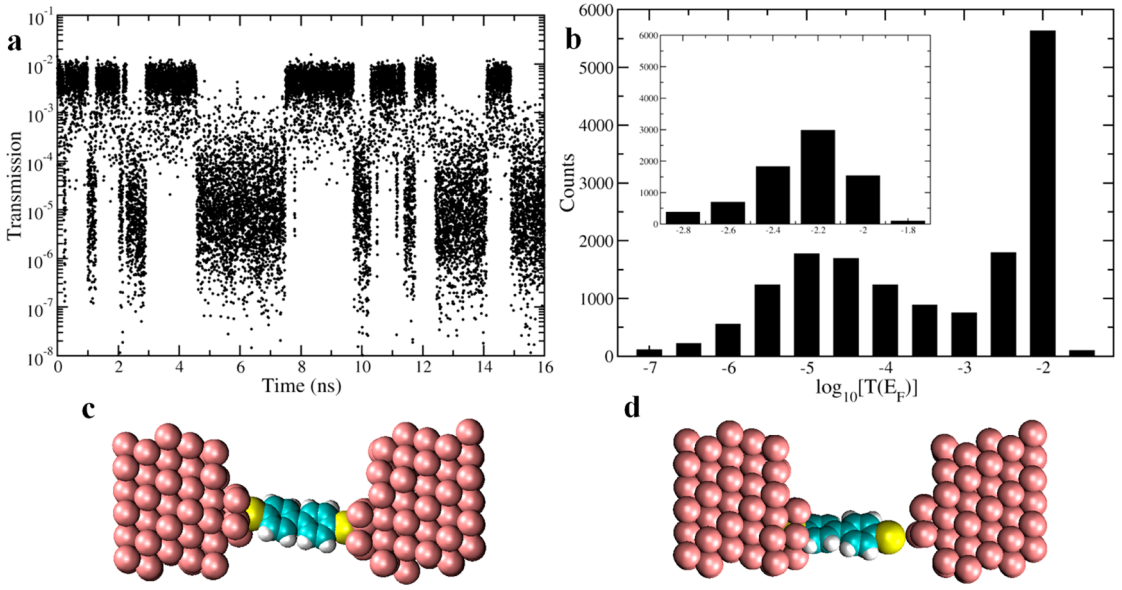

Figure 5. Transmission and geometric properties of molecular junction with disordered electrodes. (a) The time-dependent transmission exhibits distinct switching between a high-conductance and low-conductance state. (b) The log-normal histogram of transmission values is best described by a bimodal distribution, in contrast to the unimodal distribution seen in Figure 3. The source of the switching is the geometric fluctuations within the junction, shown in panels c and d. (c) The biphenyl is in the middle of the junction, adsorbed on islands of gold atoms in a high-conductance state. (d) The molecular linker is adsorbed more closely to one electrode in a low-conductance state.

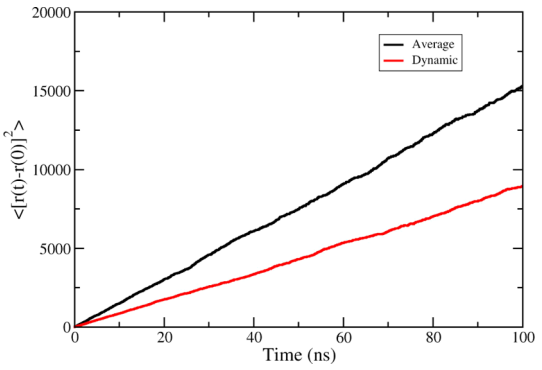

Figure 6. Electronic mean squared displacements (MSD) as a function of time for the system with disordered electrodes. As in Figure 4, the "dynamic" curve (red) is computed using the hierarchy described in Figure 2, while the "average" curve (black) is calculated assuming that all electron hopping rates are equivalent to the average hopping rate from the "dynamic" simulation. In this case, the average and dynamic curves have unequal slopes, indicating that fluctuations do affect the mesoscopic electronic motion.

do not significantly affect the mesoscopic transport. If the fluctuations occur more slowly than the characteristic hopping time, the junction becomes dynamically gated by the time-evolution of the junction geometry, and the electronic diffusion is lower than it would be for the same system with fast fluctuations.

From the MD simulations of this dynamically disordered system, we found that the times between switching times follow an exponential distribution (Supporting Information text, Figure S.1). Using this result, KMC simulations were devised in which electrons hop between nearest neighbors through a network of sites, with each junction allowed to switch between two transmission states, with the switching described by a Poisson process. Normalized electronic diffusion coefficients from these simulations are shown as points in Figure 7. An effective diffusion coefficient of 1 corresponds to diffusion where all switches are in the high-transmission state at all times, while an effective diffusion coefficient of 0 indicates no electronic diffusion.

Three parameters are varied in Figure 7: the average switching time (renewal time), the low/high-transmission ratio, and the percent of junctions that are in the high-transmission state *versus* low-transmission state. For all cases, increasing the renewal time decreases the effective diffusion. This is a result of dynamical gating of the individual junctions. For fast fluctuations (short renewal times), the effective rate reaches the weighted average value of the low-transmission (low-T) and high-transmission (high-T) states, similar to the behavior observed in the ordered electrode system. As the renewal time increases, the effective rate approaches the static percolation limit. Decreasing the transmission of the low-T junctions (blue points) enhances the percolation effect because the dynamical gating is more pronounced. The effect is particularly important when only $^1/_3$ (or fewer) of the junctions are in the high-T state (Figure 7c). This is a consequence of the system's connectivity being below the bond percolation threshold (0.347 in a hexagonal array) which results in a static percolation limit of zero when the transmission of the low-T state is zero (see Figure S.2 in Supporting Information for more details). The normalized diffusion coefficient for the system with disordered electrodes (*i.e.*, calculated from the full

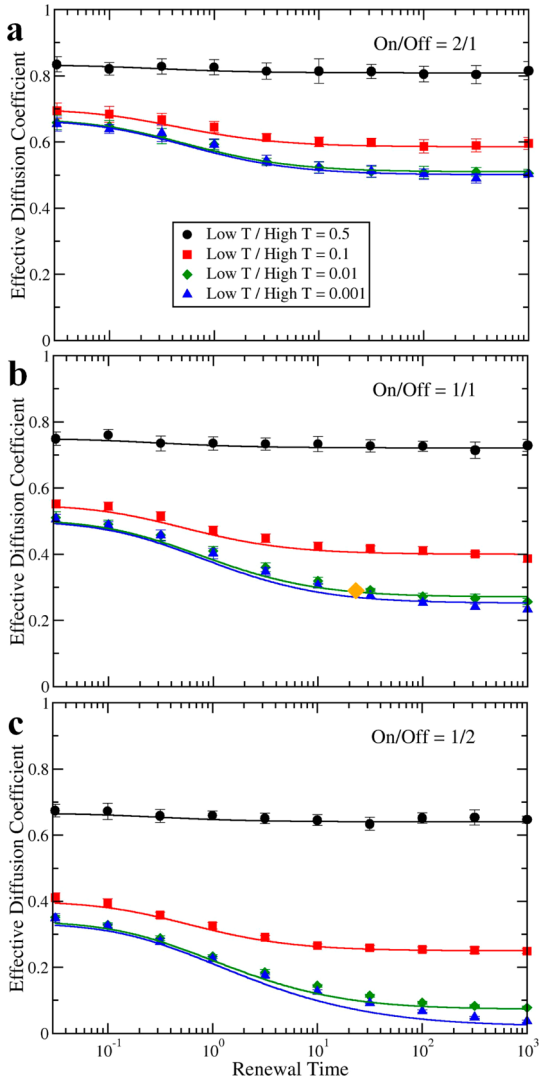

Figure 7. Diffusion coefficients vary as a function of the bond renewal time, the low/high transmission ratio, and the ratio of switches in the on/off states. Diffusion coefficients are normalized by the diffusion coefficient of a system composed entirely of bonds in the "on" state, equivalent to the system in Figure 4. Renewal times are in units of the characteristic electron hopping time across an "on" junction. In general, increasing the renewal time decreases the electronic diffusion. The orange diamond in panel b corresponds to the normalized diffusion for the system with disordered electrodes. The disordered electrode system has a low-T/high-T ratio of approximately 0.003. Error bars represent standard deviations.

multiscale approach as in Figure 6) is shown in Figure 7b (orange diamond) for comparison. There is good agreement with the simulations based on Poisson-distributed switching times, justifying the simplification.

The curves in Figure 7 are analytical solutions of the effective rate based on a dynamic effective-medium approximation.[49,50] Dynamic bond percolation theory (DBPT) was devised to describe charge carrier motion through an array of fluctuating bonds, emphasizing the importance of the bond dynamics on the carrier mobility. The rates calculated using KMC simulations and DBPT agree very well, suggesting that DBPT is an effective tool for describing the effects of dynamical gating on the relative electronic diffusion through dynamically disordered nanoparticle arrays, provided the switching events can be described by a Poisson process.

To relate the DBPT calculations with results from the hierarchical computational approach described in Figure 2, parameters are required that describe the ratio of switches in the on/off states, the high/low transmission ratio for switches in the on/off states, and the topology of the connected network. The two former parameters can be obtained from a combination of the MD simulations and transport calculations while the latter parameter is obtained assuming a hexagonally packed array. Defects in the structure of the array will change the parameter that accounts for the array topology and affect both the computational and analytical results. In this study, such defects have not been considered. Also, it should be noted that the DBPT will yield effective rates as opposed to the absolute rates that are calculated from the hierarchical approach. Additional details on DBPT are available in the Supporting Information text.

CONCLUSIONS

We have developed a multiscale computational approach to treat the problem of electronic motion through molecularly linked nanoparticle arrays. Using a combination of molecular dynamics, quantum transport calculations, and kinetic Monte Carlo simulations, we have explored the effects of geometric fluctuations on mesoscopic transport through a hybrid material. The calculations have underscored the challenges involved with modeling transport through nanostructured materials: electronic motion occurs on multiple time and length scales, and slight changes on the atomic scale can dramatically affect the charge transport properties on the mesoscopic scale. The results and accompanying analysis using dynamic mean-field theory identify the conditions under which electronic motion will be hindered by structural fluctuations in the constituent junctions. Fluctuations in the junction transmission that occur faster than the characteristic hopping time average to give results similar to conductance measurements in single molecule junctions. Slower fluctuations result in dynamical gating that will decrease the diffusivity of electrons through the array and make the individual junctions appear to be less conducting. This has important implications for extracting information about single molecule junction conductance from an interconnected nanoparticle array.

Our findings also suggest a way forward for experimental studies. Minimizing long-lived geometric fluctuations will improve the utility of nanoparticle arrays to function as test-beds for molecular electronic junctions. To accomplish this, nanoparticle surfaces should be nearly free of defects in systems with Au–S binding, a challenging prospect with current fabrication techniques. Alternatively, utilizing less labile

molecule−electrode binding motifs[27−29,38] should reduce the effects of stochastic fluctuations on the array conductance. In addition to the theoretical approach described here, recent innovations in ultrafast single-molecule conductance measurements may provide a method for examining conductance fluctuations on the nanosecond scale.[57] By combining theoretical and experimental techniques, appropriate binding motifs can be identified, and molecularly linked nanoparticle arrays can more effectively serve as architectures with which to test and develop molecular junctions.

Although the system studied here (molecular dynamic occurring in molecules whose terminal ends can bind to metallic quantum dots) has been investigated experimentally, many other situations can exist in the general area of molecular devices, in which more than one time scale is relevant for the evolution of system dynamics, structure and transport. Combining molecular dynamics with kinetic Monte Carlo and electron tunneling calculations provides a broadly applicable and physically sound approach to these multitime scale, multimotion systems.

MATERIALS AND METHODS

Molecular Dynamics. The Tinker Molecular dynamics program[58] is utilized for molecular dynamics simulations. Simulations are run in the canonical ensemble (NVT) at 300 K using the Nose-Hoover thermostat. The equations of motion are integrated using a velocity Verlet algorithm with a 1.0 fs time step. All MD runs are equilibrated for 1 ns, after which junction configurations are recorded every 1 ps for 16 ns. Buckingham potentials are used to treat interatomic interactions, and specific force field parameters are adopted from previous studies by Goddard *et al.* (see Table S.1 in Supporting Information).[59,60]

Each junction is composed of a dithiolated biphenyl bound between Au(111) electrodes with periodic boundary conditions in the plane of the electrode surfaces. The electrodes are composed of six layers of gold atoms with 18 atoms per layer. Two types of electrode surface structure are considered: one with a full layer of Au atoms on the surface (18 atoms), and one with $^2/_3$ of the surface atoms missing (leaving six surface atoms). The average interelectrode distance is set to 14.4 Å, and the average is maintained by immobilizing the three electrode layers furthest from the junction on each side. The biphenyl dithiol as well as the three surface layers nearest the junction are allowed to thermally fluctuate.

Single Junction Transport. Single molecule transport calculations are performed using Huckel-IV 2.0.[61] The Huckel-IV program calculates transport properties for a molecule bound between gold pads composed of three Au atoms each. These gold pads are then coupled to bulk electrodes. To create the pad−molecule−pad structures, every configuration in the MD trajectory is parsed to extract the coordinates of the biphenyl dithiol as well as the three gold atoms closest to each terminating sulfur atom. From these geometries, the transmission function at the Fermi energy $T(E_F)$ is calculated:

$$T(E_F) = Tr\{\Gamma^L G^{ret}(E_F)\Gamma^R G^{adv}(E_F)\} \quad (2)$$

Here, Γ^L and Γ^R are the spectral densities of the left and right leads, G^{ret} and G^{adv} are the retarded and advanced Green's functions, and E_F is the Fermi energy of bulk gold. In these calculations, the nanoparticle electrodes are treated as bulk gold, and it is assumed that coupling of the gold pads to the bulk electrodes is identical for all conformations. Additionally, we assume coherent tunneling in the low-bias limit. Under these conditions, the transmission is related to the conductance by $G = G_0{*}T(E_F)$, where G_0 is 77.5 μS.

Kinetic Monte Carlo. The KMC simulations model thermally activated electron hopping between nearest-neighbor nanoparticles assembled in a hexagonally packed 2D array. A total of 1024 nanoparticles are considered with periodic boundary conditions implemented. Electrons are assumed to be noninteracting, and only sequential tunneling is allowed. The energy difference ΔE in eq 1 is taken to be 10 meV, on the order of experimentally determined activation energies, and T in eq 1 is set to 300 K . A simulation consists of 10^5 MC steps with a time step $\Delta t = 1.0$ ps. At each Monte Carlo step, an electron may hop off particle i with a probability $P_i(t)$ given by

$$P_i(t) = 1 - e^{-k_i(t)\times\Delta t} \quad (3)$$

The overall rate to leave particle i is

$$k_i(t) = \sum_{6}^{j=1} k_{i\to j}(t) \quad (4)$$

where $k_{i\to j}(t)$ is defined in eq 1. As mentioned previously, each interparticle hopping rate changes from $k_{i\to j}(t) \to k_{i\to j}(t + \Delta t)$ after every MC step. If a bond is described by the rate $k_{i\to j}(t_f)$, the final rate in the time-dependent set $\{k\}$, then the subsequent rate will be $k_{i\to j}(t_0)$, the first value in the set $\{k\}$. In this way, the KMC simulations may span time lengths longer than the simulated MD times. Finally, diffusion coefficients are computed from the average electronic mean squared displacement:

$$D = \frac{[r(t) - r(0)]^2}{4t} \quad (5)$$

Here $r(t) - r(0)$ is the distance traveled by a hopping electron after a time interval of length t. The average in eq 5 is performed over 1024 electron trajectories.

Conflict of Interest: The authors declare no competing financial interest.

Acknowledgment. We thank the Chemistry Division of the NSF, for supporting this research through an NSF predoctoral fellowship (C.G.). This work was supported by the Nonequilibrium Energy Research Center (NERC) which is an Energy Frontier Research Center funded by the U.S. Department of Energy, Office of Science, Office of Basic Energy Sciences under Award Number DE-SC0000989. We are grateful to Abraham Nitzan for very useful discussions.

Supporting Information Available: Thermally-activated hopping rates, switching times, and force field parameters. This material is available free of charge *via* the Internet at http://pubs.acs.org.

REFERENCES AND NOTES

1. Marcus, R. A.; Sutin, N. Electron Transfers in Chemistry and Biology. *Biochim. Biophys. Acta* **1985**, *811*, 265–322.
2. Marcus, R. A. Chemical + Electrochemical Electron-Transfer Theory. *Annu. Rev. Phys. Chem.* **1964**, *15*, 155–&.
3. Devault, D. Quantum-Mechanical Tunnelling in Biological-Systems. *Q. Rev. Biophys.* **1980**, *13*, 387–564.
4. Onuchic, J. N.; Beratan, D. N.; Hopfield, J. J. Some Aspects of Electron-Transfer Reaction Dynamics. *J. Phys. Chem.* **1986**, *90*, 3707–3721.
5. Newton, M. D.; Sutin, N. Electron-Transfer Reactions in Condensed Phases. *Annu. Rev. Phys. Chem.* **1984**, *35*, 437–480.
6. Sumi, H.; Marcus, R. A. Dynamic Effects in Electron-Transfer Reactions. *J. Chem. Phys.* **1986**, *84*, 4894–4914.
7. Barbara, P. F.; Meyer, T. J.; Ratner, M. A. Contemporary Issues in Electron Transfer Research. *J. Phys. Chem.* **1996**, *100*, 13148–13168.

8. May, V.; Kühn, O. *Charge and Energy Transfer Dynamics in Molecular Systems*, 3rd, revision and enlarged ed.; Wiley-VCH: Weinheim, Germany, 2011; Vol. xix, p 562.
9. Hush, N. S. Adiabatic Theory of Outer Sphere Electron-Transfer Reactions in Solution. *Trans. Faraday. Soc.* **1961**, *57*, 557–580.
10. Whaley, K. B. *Quantum Mechanics in Chemistry*; Schatz, G. C., Ratner, M. A., Eds.; Prentice Hall: Englewood Clifs, NJ, 1993 (*Int. J. Quantum Chem*. **1996**, *57*, 1131).
11. Jortner, J. Temperature-Dependent Activation-Energy for Electron-Transfer Between Biological Molecules. *J. Chem. Phys.* **1976**, *64*, 4860–4867.
12. Marcus, R. A. Electron-Transfer Reactions in Chemistry—Theory and Experiment. *Rev. Mod. Phys.* **1993**, *65*, 599–610.
13. Bader, J. S.; Kuharski, R. A.; Chandler, D. Role of Nuclear Tunneling in Aqueous Ferrous Ferric Electron-Transfer. *J. Chem. Phys.* **1990**, *93*, 230–236.
14. Nitzan, A.; Ratner, M. A. Electron Transport in Molecular Wire Junctions. *Science* **2003**, *300*, 1384–1389.
15. Siebbeles, L. D. A.; Grozema, F. C., *Charge and Exciton Transport Through Molecular Wires*; Wiley-VCH: Weinheim, Germany, 2011.
16. Mayor, M.; Samorì, Paolo; Cacialli., Franco Functional Supramolecular Architectures for Organic Electronics and Nanotechnology. *Angew. Chem., Int. Ed.* **2011**, *50*, 7979–7981.
17. Iwamoto, M.; Kwon, Y.-S.; Lee, T. *Nanoscale Interface for Organic Electronics*; World Scientific: Singapore; Hackensack, NJ, 2011.
18. Cuevas, J. C.; Scheer, E. *Molecular Electronics: An Introduction to Theory and Experiment, Vol.* 1. World Scientific: Singapore, Hackensack, NJ, 2010.
19. Di Ventra, M. *Electrical Transport in Nanoscale Systems*; Cambridge University Press: Cambridge, 2008.
20. Joachim, C.; Gimzewski, J. K.; Aviram, A. Electronics Using Hybrid-Molecular and Mono-Molecular Devices. *Nature* **2000**, *408*, 541–548.
21. Nitzan, A. Electron Transmission through Molecules and Molecular Interfaces. *Annu. Rev. Phys. Chem.* **2001**, *52*, 681–750.
22. McCreery, R. L. Molecular Electronic Junctions. *Chem. Mater.* **2004**, *16*, 4477–4496.
23. Joachim, C.; Ratner, M. A. Molecular Electronics: Some Views on Transport Junctions and Beyond. *Proc. Natl. Acad. Sci. U.S.A.* **2005**, *102*, 8801–8808.
24. Makk, P.; Tomaszewski, D.; Martinek, J.; Balogh, Z.; Csonka, S.; Wawrzyniak, M.; Frei, M.; Venkataraman, L.; Halbritter, A. Correlation Analysis of Atomic and Single-Molecule Junction Conductance. *ACS Nano* **2012**, *6*, 3411–3423.
25. Chen, F.; Hihath, J.; Huang, Z.; Li, X.; Tao, N. J. Measurement of Single-Molecule Conductance. *Annu. Rev. Phys. Chem.* **2007**, *Vol. 58*, 535–564.
26. Landauer, R. Electrical Transport in Open and Closed Systems. *Z. Phys. B, Condens. Mater.* **1987**, *68*, 217–228.
27. Buttiker, M.; Imry, Y.; Landauer, R.; Pinhas, S. Generalized Many-Channel Conductance Formula with Application to Small Rings. *Phys. Rev. B* **1985**, *31*, 6207–6215.
28. Joachim, C.; Ratner, M. A. Molecular Electronics. *Proc. Natl. Acad. Sci. U.S.A.* **2005**, *102*, 8800–8800.
29. Datta, S. *Quantum Transport: Atom to Transistor*; Cambridge University Press: Cambridge, UK; New York, 2005.
30. Love, J. C.; Estroff, L. A.; Kriebel, J. K.; Nuzzo, R. G.; Whitesides, G. M. Self-Assembled Monolayers of Thiolates on Metals as a Form of Nanotechnology. *Chem. Rev.* **2005**, *105*, 1103–1169.
31. Zabet-Khosousi, A.; Dhirani, A. A. Charge Transport in Nanoparticle Assemblies. *Chem. Rev.* **2008**, *108*, 4072–4124.
32. Tagliazucchi, M.; Tice, D. B.; Sweeney, C. M.; Morris-Cohen, A. J.; Weiss, E. A. Ligand-Controlled Rates of Photoinduced Electron Transfer in Hybrid CdSe Nanocrystal/Poly(viologen) Films. *ACS Nano* **2011**, *5*, 9907–9917.
33. Morris-Cohen, A. J.; Frederick, M. T.; Cass, L. C.; Weiss, E. A. Simultaneous Determination of the Adsorption Constant and the Photoinduced Electron Transfer Rate for a CdS Quantum Dot−Viologen Complex with Transient Absorption Spectroscopy. *Abstr. Pap. Am. Chem. Soc.* **2011**, 242.
34. Liao, J. H.; Agustsson, J. S.; Wu, S. M.; Schonenberger, C.; Calame, M.; Leroux, Y.; Mayor, M.; Jeannin, O.; Ran, Y. F.; Liu, S. X.; *et al.* Cyclic Conductance Switching in Networks of Redox-Active Molecular Junctions. *Nano Lett.* **2010**, *10*, 759–764.
35. Liao, J. H.; Bernard, L.; Langer, M.; Schonenberger, C.; Calame, M. Reversible Formation of Molecular Junctions in Two-Dimensional Nanoparticle Arrays (vol 18, pg 2444, 2006). *Adv. Mater. (Weinheim, Germany)* **2006**, *18*, 2803–2803.
36. van der Molen, S. J.; Liao, J. H.; Kudernac, T.; Agustsson, J. S.; Bernard, L.; Calame, M.; van Wees, B. J.; Feringa, B. L.; Schonenberger, C. Light-Controlled Conductance Switching of Ordered Metal−Molecule−Metal Devices. *Nano Lett.* **2009**, *9*, 76–80.
37. Mangold, M. A.; Calame, M.; Mayor, M.; Holleitner, A. W. Resonant Photoconductance of Molecular Junctions Formed in Gold Nanoparticle Arrays. *J. Am. Chem. Soc.* **2011**, *133*, 12185–12191.
38. Chen, W. B.; Widawsky, J. R.; Vazquez, H.; Schneebeli, S. T.; Hybertsen, M. S.; Breslow, R.; Venkataraman, L. Highly Conducting pi-Conjugated Molecular Junctions Covalently Bonded to Gold Electrodes. *J. Am. Chem. Soc.* **2011**, *133*, 17160–17163.
39. Hong, W.; Manrique, D. Z.; Moreno-Garcia, P.; Gulcur, M.; Mishchenko, A.; Lambert, C. J.; Bryce, M. R.; Wandlowski, T. Single Molecular Conductance of Tolanes: Experimental and Theoretical Study on the Junction Evolution Dependent on the Anchoring Group. *J. Am. Chem. Soc.* **2012**, *134*, 2292–2304.
40. Hybertsen, M. S.; Venkataraman, L.; Klare, J. E.; Cwhalley, A.; Steigerwald, M. L.; Nuckolls, C. Amine-Linked Single-Molecule Circuits: Systematic Trends Across Molecular Families. *J. Phys. Condens. Mater.* **2008**, *20*, 374115.
41. Moth-Poulsen, K.; Bjornholm, T. From Nanofabrication to Self-fabrication—Tailored Chemistry for Control of Single Molecule Electronic Devices. *Chimia* **2010**, *64*, 404–408.
42. Blunt, M. O.; Suvakov, M.; Pulizzi, F.; Martin, C. P.; Pauliac-Vaujour, E.; Stannard, A.; Rushforth, A. W.; Tadic, B.; Moriarty, P. Charge Transport in Cellular Nanoparticle Networks: Meandering Through Nanoscale Mazes. *Nano Lett.* **2007**, *7*, 855–860.
43. Suvakov, M.; Tadic, B. Modeling Collective Charge Transport in Nanoparticle Assemblies. *J. Phys-Condens. Mat.* **2010**, *22*, 163201.
44. Basch, H.; Cohen, R.; Ratner, M. A. Interface Geometry and Molecular Junction Conductance: Geometric Fluctuation and Stochastic Switching. *Nano Lett.* **2005**, *5*, 1668–1675.
45. Moore, A. M.; Dameron, A. A.; Mantooth, B. A.; Smith, R. K.; Fuchs, D. J.; Ciszek, J. W.; Maya, F.; Yao, Y. X.; Tour, J. M.; Weiss, P. S. Molecular Engineering and Measurements to Test Hypothesized Mechanisms in Single Molecule Conductance Switching. *J. Am. Chem. Soc.* **2006**, *128*, 1959–1967.
46. Wassel, R. A.; Fuierer, R. R.; Kim, N. J.; Gorman, C. B. Stochastic Variation in Conductance on the Nanometer Scale: A General Phenomenon. *Nano Lett.* **2003**, *3*, 1617–1620.
47. Patrone, L.; Soullier, J.; Martin, P. Role of S−Au Labile Bonding in Stochastic Switching of Molecular Conductance Studied by STM. *Phys. Status. Solidi. B* **2010**, *247*, 1867–1870.
48. Ramachandran, G. K.; Hopson, T. J.; Rawlett, A. M.; Nagahara, L. A.; Primak, A.; Lindsay, S. M. A Bond-Fluctuation Mechanism for Stochastic Switchingin Wired Molecules. *Science* **2003**, *300*, 1413–1416.
49. Druger, S. D.; Ratner, M. A.; Nitzan, A. Polymeric Solid Electrolytes—Dynamic Bond Percolation and Free-Volume Models for Diffusion. *Solid State Ionics* **1983**, *9−10*, 1115–1120.
50. Harrison, A. K.; Zwanzig, R. Transport on a Dynamically Disordered Lattice. *Phys. Rev. A* **1985**, *32*, 1072–1075.

51. Haiss, W.; Martín, S.; Leary, E.; Zalinge, H. v.; Higgins, S. J.; Bouffier, L.; Nichols, R. J. Impact of Junction Formation Method and Surface Roughness on Single Molecule Conductance. *J. Phys. Chem. C* **2009**, *113*, 5823–5833.
52. Andrews, D. Q.; Van Duyne, R. P.; Ratner, M. A. Stochastic Modulation in Molecular Electronic Transport Junctions: Molecular Dynamics Coupled with Charge Transport Calculations. *Nano Lett.* **2008**, *8*, 1120–1126.
53. Haiss, W.; Wang, C.; Jitchati, R.; Grace, I.; Martin, S.; Batsanov, A. S.; Higgins, S. J.; Bryce, M. R.; Lambert, C. J.; Jensen, P. S.; *et al.* Variable Contact Gap Single-Molecule Conductance Determination for a Series of Conjugated Molecular Bridges. *J. Phys., Condens. Mater.* **2008**, *20*, 374119.
54. Mishchenko, A.; Vonlanthen, D.; Meded, V.; Burkle, M.; Li, C.; Pobelov, I. V.; Bagrets, A.; Viljas, J. K.; Pauly, F.; Evers, F.; *et al.* Influence of Conformation on Conductance of Biphenyl-Dithiol Single-Molecule Contacts. *Nano Lett.* **2010**, *10*, 156–163.
55. Gonzalez, M. T.; Wu, S. M.; Huber, R.; van der Molen, S. J.; Schonenberger, C.; Calame, M. Electrical Conductance of Molecular Junctions by a Robust Statistical Analysis. *Nano Lett.* **2006**, *6*, 2238–2242.
56. Kim, H. S.; Kim, Y. H. Conformational and Conductance Fluctuations in a Single-Molecule Junction: Multiscale Computational Study. *Phys. Rev. B* **2010**, 82.
57. Guo, S. Y.; Hihath, J.; Tao, N. J. Breakdown of Atomic-Sized Metallic Contacts Measured on Nanosecond Scale. *Nano Lett.* **2011**, *11*, 927–933.
58. Ponder, J. W. *Tinker 5.1*; Washington University School of Medicine: St. Louis, MO, 2010.
59. Jang, S. S.; Jang, Y. H.; Kim, Y. H.; Goddard, W. A.; Flood, A. H.; Laursen, B. W.; Tseng, H. R.; Stoddart, J. F.; Jeppesen, J. O.; Choi, J. W.; *et al.* Structures and Properties of Self-Assembled Monolayers of Bistable 2 Rotaxanes on Au(111) Surfaces from Molecular Dynamics Simulations Validated with Experiment. *J. Am. Chem. Soc.* **2005**, *127*, 1563–1575.
60. Jang, Y. H.; Jang, S. S.; Goddard, W. A. Molecular Dynamics Simulation Study on a Monolayer of Half 2 Rotaxane Self-Assembled on Au(111). *J. Am. Chem. Soc.* **2005**, *127*, 4959–4964.
61. Zahid, F.; Paulsson, M.; Datta, S. Electrical Conduction Through Molecules. *Advanced Semiconductors and Organic Nanotechniques*; Academic Press: San Diego, CA, 2003; pp 1−41.